1

Title

Mechanism of Electrolytic Reduction of SiO_2 at Liquid Zn Cathode in Molten $CaCl_2$

Authors

Yuanjia Ma[1], Akifumi Ido[2], Kouji Yasuda[2, 3, *], Rika Hagiwara[2, *], Takayuki Homma[4, *],

Toshiyuki Nohira[1, *, Z]

Affiliations

[1]Institute of Advanced Energy, Kyoto University, Gokasho, Uji, Kyoto 611-0011, Japan

[2]Graduate School of Energy Science, Kyoto University, Yoshida-honmachi, Sakyo-ku,

Kyoto 606-8501, Japan

[3]Agency for Health, Safety and Environment, Yoshida-honmachi, Sakyo-ku, Kyoto

606-8501, Japan

[4]Faculty of Science and Engineering, Waseda University, 3-4-1 Okubo, Shinjuku-ku,

Tokyo 169-8555, Japan

[*]Electrochemical Society Active Member.

[Z]Corresponding author: nohira.toshiyuki.8r@kyoto-u.ac.jp

19

Abstract

The reaction mechanism of electrolytic reduction of SiO_2 at a liquid Zn cathode in molten $CaCl_2$ was investigated with the aim of establishing a new production process of solar-grade Si. Three types of Zn/SiO_2 contacting electrodes were prepared depending on the objectives. Cyclic voltammetry suggested two reduction mechanisms of SiO_2 at a Zn electrode. One is a direct electrolytic reduction that proceeds at potentials more negative than 1.55 V vs. Ca^{2+}/Ca. The other is an indirect reduction by liquid Ca–Zn alloy at potentials more negative than 0.85 V. The both reduction mechanisms were confirmed to proceed at 0.60 V by electrolysis and immersion experiments. Impurity analysis by ICP-AES was conducted for the Si prepared by potentiostatic electrolysis at 0.60 V, and confirmed that the concentrations of the metal elements and P were lower than the target levels for primary Si before directional solidification process.

1. Introduction

Photovoltaic (PV) power generation has attracted attention as a source of green energy that can substitute the conventional fossil-based energy. The global production of

37   PV cells has experienced a rapid growth in the last decade. Accordingly, their

38   production volume increased in the 21st century by a factor of approximately 250 i.e.,

39   from 0.285 GW in 2000 to 75.5 GW in 2016. Among the many types of solar cells,

40   crystalline Si solar cells accounted for 94.3% of the worldwide production in 2016[1]. The

41   global production of high-purity crystalline Si also increased to 412,600 tons in 2016

42   i.e., by a factor of approximately 18 over the level achieved in 2000[2]. Therefore,

43   crystalline Si solar cells would most likely remain the main product of the PV industry

44   in the long term.

45   The high-purity Si used in crystalline Si solar cells is known as solar-grade Si

46   (SOG-Si), and requires a purity of 6–7N. Approximately 90% of SOG-Si is currently

47   produced by the Siemens process[3–5]. To develop a next-generation production process

48   for SOG-Si, purification of metallurgical-grade Si[6–11] and metallothermic reduction of

49   silicon halides by metal reductants[12–15] were investigated. One of the metallothermic

50   reduction processes proposed is a reduction of $SiCl_4$ by Zn, and is known as the Du Pont

51   process, which was the commercial process for high-purity Si production before the

52   Siemens process was introduced[12]. There are two major advantages of the Du Pont

53   process. One is no formation of Si–Zn intermetallic compounds due to the low chemical

54   affinity of Zn with Si[16]. The other is the easy removal of the unreacted Zn and $ZnCl_2$

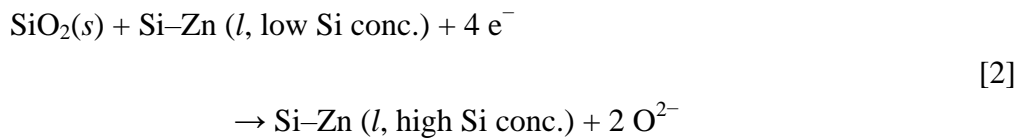55   generated from the Si product because of their high vapor pressures.

56   For the past two decades, we have been studying the direct electrolytic

57   reduction of solid SiO_2 to Si in molten $CaCl_2$ as a new production process of SOG-Si[17–

58   20]. Here, since purification of SiO_2 up to 6-7N is possible at low cost[21,22], such purified

59   SiO_2 is assumed to be used as the raw material[22]. In this process, electrochemical

60   reduction of insulating SiO_2 is realized by using a SiO_2 contacting electrode, which

61   provides the three-phase zone of conductor/SiO_2/$CaCl_2$[17].

$$SiO_2(s) + 4\ e^- \rightarrow Si(s) + 2\ O^{2-} \qquad [1]$$

62   Several other research groups have also investigated the direct electrolytic reduction of

63   SiO_2[23–34]. One of the challenges faced in the industrial application of this process is the

64   efficient recovery and separation of the powdery Si product from unreacted SiO_2 and

65   molten $CaCl_2$[35].

66   Recently, we proposed an electrolytic reduction process of SiO_2 using a liquid

67   Zn cathode in molten $CaCl_2$. Since the electrolysis product is liquid Si–Zn alloy, its

68   separation from unreacted SiO_2 and molten salt is expected to be easier than that

69   entailed in the use of the conventional solid cathode[36, 37]. The choice of Zn as an

70   alloying element stems from the very factors that render the Du Pont process

71   advantageous, i.e., the use of Zn ensures the formation of no intermetallic compounds

72   with Si, and facilitates easy removal of both Zn and $ZnCl_2$. Here, the most important

73   point is that the existence of molten salt over liquid Zn effectively suppresses the

74   evaporation of Zn even at high temperatures such as 1123 K. Figure 1 schematically

75   illustrates the proposed process[36, 37]. The overall process consists of three major steps:

76   electrolysis, precipitation, and refining. In the electrolysis step, solid SiO_2 is reduced to

77   form liquid Si–Zn alloy at a liquid Zn cathode.

$$SiO_2(s) + \text{Si–Zn } (l, \text{ low Si conc.}) + 4 \text{ e}^-$$
$$\rightarrow \text{Si–Zn } (l, \text{ high Si conc.}) + 2 \text{ O}^{2-} \tag{2}$$

78   In the precipitation step, solid Si is recovered by lowering the temperature of the liquid

79   Si–Zn alloy.

$$\text{Si–Zn } (l, \text{ high Si conc.}) \rightarrow Si(s) + \text{Si–Zn } (l, \text{ low Si conc.}) \tag{3}$$
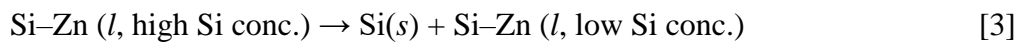
80   Since the solubility of Si in liquid Zn is 6 at.% at 1123 K and 1 at.% at 923 K[38], 5 at.%

81   of solid Si with reference to Zn is theoretically recovered when the temperature is

82   lowered from 1123 K to 923 K. After the precipitation step, the Si–Zn alloy with a low

83   concentration of Si is reused as the cathode in the electrolysis step. The Si recovered is

84   then subjected to the refining step: that entails vacuum refining to remove residual Zn

85   and directional solidification to manufacture SOG-Si ingots.

86   In our previous study, the suppression of evaporation of Zn metal by covering it

87 with molten $CaCl_2$ was confirmed at 1123 K[36, 37]. Moreover, the alloying rate between

88 solid Si and liquid Zn was measured, and the formation of liquid Si–Zn alloy at a liquid

89 Zn cathode was demonstrated[36, 37]. After potentiostatic electrolysis at 0.9 V, Si particles

90 of sizes in the range 2–30 μm were precipitated in the solidified Zn matrix. The

91 formation of liquid Ca–Zn alloy (reaction [4]) was also suggested by cyclic

92 voltammetry.

$$Zn(l) + Ca^{2+} + 2\ e^- \rightarrow Ca\text{–}Zn(l) \qquad [4]$$

93 Based on these results, the electrolytic reduction of SiO_2 at a liquid Zn cathode was

94 considered to be a mixed mechanism of (A) direct electrolytic reduction of SiO_2

95 (reaction [5]), and (B) indirect reduction of SiO_2 by liquid Ca–Zn alloy (reaction [6]).

$$SiO_2(s) + Zn(l) + 4\ e^- \rightarrow Si\text{–}Zn(l) + 2\ O^{2-} \qquad [5]$$

$$SiO_2(s) + Ca\text{–}Zn(l) \rightarrow Si\text{–}Zn(l) + 2\ CaO(l) \qquad [6]$$

96 However, the evidence of (B) i.e., indirect reduction was not seen, and the contributions

97 of (A) and (B) were not investigated.

98   In the present study, a series of electrolysis and immersion experiments were

99 conducted to confirm the indirect reduction of SiO_2. Based on the results, the mixed

100 reduction mechanism was discussed in terms of reduction rate. Finally, impurity

101 analysis was performed for the Si particles produced at the Zn cathode.

102

2. Experimental

All experiments were performed in a dry Ar atmosphere at 1123 K. An Ag^+/Ag electrode was used as the reference electrode in the experiments. The experimental conditions for (a) cyclic voltammetry, (b) electrolytic reduction of SiO_2 plates, and (c) electrolytic reduction of SiO_2 particles are described below.

(a) Cyclic Voltammetry

Figure 2 shows a schematic illustration of the electrolysis cell for the observation of the reduction behavior of SiO_2 at a liquid Zn cathode. Figure 3(a) schematically illustrates the structure of the liquid Zn working electrode for cyclic voltammetry. Approximately 70 g of Zn (Wako Pure Chemical Corp., reagent grade, granule) was charged into a small Al_2O_3 crucible (AS ONE, o.d. 45 mm × height 36 mm, >99%). The small Al_2O_3 crucible was placed at the bottom of another Al_2O_3 crucible (AS ONE, o.d. 90 mm × i.d. 80 mm × height 140 mm, >99%), and approximately 500 g of $CaCl_2$ (Kojundo Chemical Laboratory Co., Ltd., >99%) was charged. A W wire (The Nilaco Corporation, diameter 2.0 mm, 99.95%) threaded into an Al_2O_3 tube (Nikkato Corp., SSA-S grade, o.d. 6.0 mm × i.d. 4.0 mm) or a SiO_2 tube (Soei Riken Corp., o.d.

120   6.0 mm × i.d. 2.0 mm) was used as the current lead and immersed in the liquid Zn in the

121   small Al_2O_3 crucible. The direct electrolytic reduction of SiO_2 occurs at the three-phase

122   interface of (Al_2O_3 or SiO_2)/$CaCl_2$ (l)/Zn (l), as shown in Fig. 3(a). For comparison, a

123   square-shaped plate of single-crystal Si (ca. 30 mm × 5 mm × 0.5 mm, p-type, (100),

124   1.5–3.0 × 10^{-3} Ω cm at 298 K) was also used as the working electrode. The counter

125   electrode was a square graphite bar (Toyo Tanso Co., Ltd., 5 mm × 5 mm × height 50

126   mm).

127

128   (b) Electrolytic reduction of SiO_2 plates

129   Figure 3(b) shows a schematic illustration of the liquid Zn cathode for the

130   investigation of the effect of indirect reduction of SiO_2 by liquid Ca–Zn alloy.

131   Approximately 125 g of Zn was charged into a small ZrO_2 crucible (AS ONE, ZrO_2

132   91.5%, Y_2O_3 8%, o.d. 60 mm × i.d. 52 mm × height 35 mm). The ZrO_2 crucible was

133   placed in a graphite crucible (Toyo Tanso Co., Ltd., IG-110 grade, o.d. 100 mm × i.d. 90

134   mm × height 120 mm) to which a graphite rod (Toyo Tanso Co., Ltd., IG-110 grade,

135   diameter 9 mm) was fixed using a stainless steel screw. Approximately 500 g of $CaCl_2$

136   was charged into the graphite crucible. A SiO_2 plate (Soei Riken Corp., 25 mm × 10 mm

137   × thickness 1 mm), fixed to an insulating tube of Al_2O_3 (Nikkato Corp., SSA-S grade,

138   o.d. 2.5 mm × i.d. 1.5 mm) by winding a Mo wire (The Nilaco Corporation, diameter

139   0.20 mm, 99.95%), was immersed into the liquid Zn in the small ZrO_2 crucible. The

140   counter electrode was the graphite crucible, and the graphite rod was used as the current

141   lead. The test piece prepared by electrolysis or immersion of SiO_2 plate was washed

142   with distilled water to remove the salt, and then immersed in HCl aq. (3 wt.%, prepared

143   from Fujifilm Wako Pure Chemical Corporation, reagent grade, 36 wt.%) overnight to

144   dissolve the Zn metal on the surface of the plate. An optical microscope (Thanko Inc.,

145   DILITE30) was used for surface observation, and the masses of the SiO_2 plates were

146   measured before and after the experiment.

147

148   (c) Electrolytic reduction of SiO_2 particles

149   Figure 4 schematically illustrates a cell for the electrolytic reduction of SiO_2

150   particles. A total of 335 g of Zn and 349 g of $CaCl_2$ were charged into an Al_2O_3 crucible.

151   After the temperature was raised to 1123 K, a total of 16.2 g of SiO_2 particles (Kojundo

152   Chemical Laboratory Co., Ltd., 0.25−1.00 mm, 99.995%) was charged into molten salt

153   uniformly using a quartz funnel. The SiO_2 particles floated on the surface of liquid Zn in

154   molten $CaCl_2$ because the densities of liquid $CaCl_2$, solid SiO_2, and liquid Zn are 2.05 g

155   cm^{-3}, 2.2 g cm^{-3}, and 5.9 g cm^{-3}, respectively, at 1123 K. A W wire (The Nilaco

156 Corporation, diameter 1.0 mm, 99.95%) threaded into an alumina tube was used as the

157 current lead for liquid Zn. The counter electrode was a graphite rod (Toyo Tanso Co.,

158 Ltd., IG-110 grade, diameter 20 mm × height 40 mm) fixed to a thinner graphite rod

159 (Toyo Tanso Co., Ltd., IG-110 grade, diameter 9 mm × height 500 mm). The sample

160 obtained after electrolysis was cooled from 1123 K to 773 K for 35 h, then maintained

161 at 773 K for 10 h, and further cooled to 298 K for 5 h. The ingot of Zn metal was

162 recovered after the removal of $CaCl_2$ by flowing water. The Zn metal ingot was

163 dissolved in HCl aq. (20 wt.%). The particles recovered after the dissolution of HCl

164 were further washed; they were alternately immersed in HCl aq. (10 wt.%) twice and in

165 HF aq. (5 wt.%, prepared from Tama Chemicals Co., Ltd., AA-100 grade, 38 wt.%)

166 once overnight. The analysis was conducted using X-ray diffraction (XRD, Rigaku,

167 Ultima 4, Cu-$K\alpha$, λ = 1.5418 Å, 40 kV, 40 mA) and inductively coupled plasma atomic

168 emission spectroscopy (ICP-AES; AMETEK, Inc., SPECTROBLUE).

169

170 **3. Result and Discussion**

171 (a) Cyclic Voltammetry

172 Figure 5 shows the cyclic voltammograms at the liquid Zn (black color) and Si

173 plate (red color) electrodes. As for the Si electrode, the cathodic and anodic current

174   peaks at around 1.3–1.4 V vs. Ca^{2+}/Ca correspond to the reduction of surface SiO_2 film

175   to metallic Si and the oxidation of Si into SiO_2 layer, respectively[35, 39]. The smaller

176   anodic current compared with the cathodic current is due to the passivation effect of the

177   formed SiO_2 layer. The redox at 0.5 V is attributed to $CaSi_2/Si$[35, 39]. The solid and

178   broken black lines show the voltammograms at Zn electrodes using Al_2O_3 and SiO_2

179   tubes, respectively. A sharp increase in cathodic current at 0.85 V is seen at both the Zn

180   electrodes. Since the electrochemical reduction of Al_2O_3 does not occur in the potential

181   range measured[40], the cathodic current is attributed to the formation of liquid Ca–Zn

182   alloy, which was already confirmed by potentiostatic electrolysis at potentials more

183   negative than 0.85 V[37]. In the case of the Zn electrode with SiO_2, the rest potential is

184   1.55 V, which is more positive than that of the Si plate electrode (1.47 V), and the

185   cathodic current is observed from the rest potential in the negative scan even at

186   potentials more positive than 1.3 V. These results suggest the formation of liquid Si–Zn

187   alloy with Si activity lower than unity with respect to pure solid Si. The cathodic current

188   at the Zn electrode with SiO_2 was 80 mA larger than that with Al_2O_3, which also

189   suggests electrolytic reduction of SiO_2 (reaction [5]).

190

191   (b) Electrolytic reduction of SiO_2 plates

192   On the basis of the voltammetry results, potentiostatic electrolysis was first

193   conducted at 0.60 V and then at 0.90 V. Specifically, the experiments were conducted in

194   the following order: [A1] electrolysis at 0.90 V for 30 min, [B1] immersion for 30 min,

195   [A2] electrolysis at 0.60 V for 30 min, and [B2] immersion for 30 min. Here, a new

196   SiO_2 plate was used in each step. As a result, four samples, A1, B1, A2 and B2, were

197   prepared. Since electrolysis was not conducted for the samples B1 and B2, the reduction

198   of SiO_2 could be advanced only due to indirect reduction by liquid Ca–Zn alloy

199   (reaction [6]). On the other hand, the reduction of the samples A1 and A2 could proceed

200   by a mixed reduction mechanism comprising direct electrolytic reaction (reaction [5])

201   and indirect reduction by liquid Ca–Zn alloy.

202   The optical images of the samples A1, B1, A2, and B2 are shown in Figure 6.

203   For the sample A1, which was electrolyzed at 0.90 V, a change in color from transparent

204   i.e., no color to dark brown is observed in a portion lower than the $Zn/CaCl_2$ interface (8

205   mm from the bottom of the SiO_2 plate). Also, a decrease in plate thickness is clearly

206   observed. In the case of the sample A2, which was electrolyzed at 0.60 V, the entire area

207   below the $Zn/CaCl_2$ interface changed to dark brown in color. In this case, the plate

208   became thinner, showing that a larger amount of the Si–Zn liquid alloy was produced.

209   The thickness was more decreased near the three-phase interface of $Zn/SiO_2/CaCl_2$ in

comparison with the two-phase interface of Zn/SiO_2 in liquid Zn. This is explained by higher solubility and faster diffusion of O^{2-} ions in molten $CaCl_2$ compared with those in liquid Zn. As for the immersion sample B1, no dark brown part is observed, indicating no progress of indirect reduction. Concerning the sample B2, which was immersed after electrolysis at 0.60 V, the color of the immersed portion changed to dark brown. This is explained by the indirect reduction. The weight losses of the samples were 0.03 g (A1), 0.07 g (A2), 0.00 g (B1), and 0.03 g (B2).

By comparing the samples A1 and B1, it can be inferred that only the direct reduction of SiO_2 (reaction [5]) occurs at 0.90 V. On the other hand, the results for sample A2 and B2 conclude that comparable amount of reduction proceeded in the indirect reaction, i.e., reduction by liquid Ca–Zn alloy (reaction [6]), in the electrolysis at 0.60 V to the direct reduction.

(c) Electrolytic reduction of SiO_2 particles

To prepare a sample for impurity analysis, potentiostatic electrolysis of SiO_2 particles was conducted at 0.60 V for 50 h. Figure 7(a) shows a photograph of the granules recovered after the dissolution of Zn by HCl solution and the treatment of acid washing. The XRD analysis confirms that the granules are crystalline Si (Figure 7(b)).

228   The current efficiency (η) is calculated by the following equations:

$$\eta = \frac{W_{act.}}{W_{theo.}} \times 100 \tag{7}$$

$$W_{theo.} = \frac{Q}{4\,F} \times M_{Si} \tag{8}$$

229   where Q is the quantity of electric charge during electrolysis, F is Faraday's constant

230   (96485 C mol^{-1}), M_{Si} is the molar weight of Si (28.1 g mol^{-1}), $W_{act.}$ is the actual weight

231   of the Si recovered, and $W_{theo.}$ is the theoretical weight of Si by Faraday's law in

232   reaction [5]. From the values of $W_{act.}$ = 3.02 g and $Q = 1.48 \times 10^5$ C, η is calculated to

233   be 28%. One of the reasons for the low current efficiency is the loss during acid

234   washing. Another is the formation of liquid Ca–Zn alloy as a side reaction; a part of it

235   contributes to the indirect reduction of SiO_2 and the other remains as Ca–Zn alloy.

236   Table 1 lists the impurity contents of the Si granules after the treatment of acid

237   washing. It also lists the acceptable levels for SOG-Si[41], segregation coefficients[7], and

238   target levels for primary Si for directional solidification. For comparison, the impurity

239   contents of the Si sample obtained by solid electrolytic reduction at 0.60 V for 5 h in

240   molten $CaCl_2$ are also shown[42]. The impurity levels of the metallic elements (Al, Ca, Fe,

241   and Ti) in the Si granules meet the target levels for the primary Si that is to be further

242   purified by unidirectional solidification according to the process proposed in Figure 1.

243   The content of P is also lower than the target level for the primary Si, and this is

244 noteworthy because the removal of P from elemental Si is known to be difficult. The

245 content of B is higher than the target level, and this needs to be improved in the future.

246 Overall, a comparison between the impurity concentrations in the Si products obtained

247 by electrolysis at a liquid Zn cathode and at a solid electrode indicates that higher purity

248 is achieved by the use of the liquid Zn electrode. The main reason for the higher purity

249 is the solidification refining during the precipitation of Si from the Si–Zn alloy wherein

250 most impurities remain in the liquid Zn phase. It should be mentioned that the Ca

251 concentration is lower than the target level for the primary Si in spite of the use of

252 indirect reduction by liquid Ca–Zn at 0.60 V. Calcium is also expected to be removed to

253 the Zn phase during precipitation. Although a relatively large amount of Zn (6055

254 ppmw) remained in the Si granules, this can be easily removed in the gas phase during

255 the refining process owing to its high vapor pressure.

256

257 **4. Conclusion**

258   The reaction mechanism of electrolytic reduction of SiO_2 at a liquid Zn cathode

259 was investigated in molten $CaCl_2$ at 1123 K. Cyclic voltammetry suggested that

260 electrolytic reduction of SiO_2 started from the rest potential (1.55 V), and liquid Ca–Zn

261 alloy was formed at potentials more negative than 0.85 V. The progress of the indirect

262 reduction of SiO_2 by liquid Ca–Zn alloy was confirmed by electrolysis and immersion

263 experiments. The reduction at 0.60 V proceeded by a mixed reduction mechanism of

264 direct electrolytic reaction and indirect reduction by Ca–Zn alloy. Impurity analysis

265 confirmed that the concentrations of the metal elements and P were lower than the target

266 levels for primary Si. The indirect reduction of SiO_2 by liquid Ca–Zn does not increase

267 the Ca content of the Si product because it is removed to the Zn phase during

268 precipitation.

269

277

278 **References**

279 1. *Photovoltaic Market 2017*, RTS Corp. (2017). [in Japanese]
280 2. *Industrial Rare Metal 2017*, Arumu Publ. Co. (2017).

281   3.   H. Schweickert, K. Reusche and H. Gustsche, U.S. Patent 3011877, (1961).

282   4.   H. Gutsche, U.S. Patent 3011877, (1962).

283   5.   C. Bye and B. Ceccaroli, *Sol. Energ. Mater. Sol. C.*, **130**, 634 (2014).

284   6.   G. Burns, J. Rabe and S. Yilmaz, PCT International Patent WO2005/061383,
285   (2005).

286   7.   F. A. Trumbore, *Bell Syst. Tech. J.*, **39**, 205 (1959).

287   8.   X. Ma, T. Yoshikawa and K. Morita, *Sep. Purif. Technol.*, **125**, 264 (2014).

288   9.   Y. Wang, X. Ma and K. Morita, *Metall. Mater. Trans. B*, **45**, 334 (2014).

289   10.   K. Tang, S. Andersson, E. Nordstrand and M. Tangstad, *JOM*, **64**, 952 (2012).

290   11.   K. Hanazawa, N. Yuge and Y. Kato, *Mater. Trans.*, **45**, 844 (2004).

291   12.   D. W. Lyon, C. M. Olson and E. D. Lewis, *J. Electrochem. Soc.*, **96**, 359 (1949).

292   13.   S. Yoshizawa, T. Hatano and S. Sakaguchi, *Kogyo Kagaku Zasshi*, **64**, 1347
293   (1961). [in Japanese]

294   14.   J. M. Blocher, Jr., M. F. Browning and D. A. Seifert, DOE/JPL Report
295   954339-81/21 (1981).

296   15.   A. Sanjurjo, PCT International Patent WO1983/002443, (1983).

297   16.   T. B. Massalski, H. Okamoto, P. R. Subramanian and L. Kacprzak, *Binary Alloy*
298   *Phase Diagrams, 2nd ed.*, ASM International, Metals Park, Ohio, USA (1990).

299   17.   T. Nohira, K. Yasuda and Y. Ito, *Nat. Mater.*, **2**, 397 (2003).

300   18.   K. Yasuda, T. Nohira, K. Amezawa, Y. H. Ogata and Y. Ito, *J. Electrochem. Soc.*,
301   **152**, D69 (2005).

302   19.   K. Yasuda, T. Nohira, R. Hagiwara and Y. H. Ogata, *Electrochim. Acta*, **53**, 106
303   (2007).

304   20.   T. Nohira, *Yoyuen Oyobi Koon Kagaku*, **54**, 95 (2011). [in Japanese]

305   21.   M. Bessho, Y. Fukunaka, H. Kusuda and T. Nishiyama, *Energy Fuels*, **23**, 4160
306   (2009).

307   22.   T. Homma, N. Matsuo, X. Ynag, K. Yasuda, Y. Fukunaka and T. Nohira,
308   *Electrochim. Acta*, **179**, 512 (2015).

309   23.   X. Jin, P. Gao, D. Wang, X. Hu and G. Z. Chen, *Angew. Chem. Int. Ed.*, **43**, 733
310   (2004).

311   24.   P. C. Pistorius and D. J. Fray, *J. SAIMM*, **106**, 31 (2006).

312   25.   S. Lee, J. Hur and C. Seo, *J. Ind. Eng. Chem.*, **14**, 651 (2008).

313   26.   J. Yang, S. Lu, S. Kan, X. Zhang and J. Du, *Chem. Commun.*, 3273 (2009).

314   27.   E. Juzeliunas, A. Cox and D. J. Fray, *Electrochem. Commun.*, **12**, 1270 (2010).

315   28.   W. Xiao, X. Jin, Y. Deng, D. Wang and G. Z. Chen, *J. Electroanal. Chem.*, **639**,
316   130 (2010).

317   29.   E. Ergül, İ. Karakaya and M. Erdoğan, *J. Alloy. Compd.*, **509**, 899 (2011).

318   30.   S. Cho, F. F. Fan and A. J. Bard, *Electrochim. Acta*, **65**, 57 (2012).

319   31.   H. Nishihara, T. Suzuki, H. Itoi, B. An, S. Iwamura, R. Berenguer and T. Kyotani,
320   *Nanoscale*, **6**, 10574 (2014).

321   32.   S. Fang, H. Wang, J. Yang, S. Lu, B. Yu, J. Wang and C. Zhao, *Mater. Lett.*, **160**, 1
322   (2015).

323   33.   S. Fang, H. Wang, J. Yang, S. Lu, B. Yu, J. Wang and C. Zhao, *Rare Metal*, **89**, 1
324   (2016).

325   34.   S. Fang, H. Wang, J. Yang, S. Lu, B. Yu, J. Wang and C. Zhao, *J. Phys. Chem.*
326   *Solids*, **89**, 1 (2016).

327   35.   T. Toba, K. Yasuda, T. Nohira, X. Yang, R. Hagiwara, K. Ichitsubo, K. Masuda
328   and T. Homma, *Electrochemistry*, **81**, 559 (2013).

329   36.   T. Nohira, A. Ido, T. Shimao, X. Yang, K. Yasuda, R. Hagiwara and T. Homma,
330   *ECS Trans.*, **75**, 17 (2016).

331   37.   K. Yasuda, T. Shimao, R. Hagiwara, T. Homma and T. Nohira, *J. Electrochem.*
332   *Soc.*, **164**, H5049 (2017).

333   38.   R. W. Olensinski and G. J. Abbaschian, *Bull. Alloy Phase Diagr.*, **5**, 271 (1984).

334   39.   K. Yasuda, T. Nohira and Y. Ito, *J. Phys. Chem. Solids*, **66**, 443 (2005).

335   40.   H. Kadowaki, Y. Katasho, K. Yasuda and T. Nohira, *J. Electrochem. Soc.*, **165**,
336   D83 (2018).

337   41.   N. Yuge, M. Abe, K. Hanazawa, H. Baba, N. Nakamura, Y. Kato, Y. Sakaguchi, S.
338   Hiwasa and F. Aratani, *Prog. Photovolt. Res. Appl.*, **9**, 203 (2001).

339   42.   X. Yang, K. Yasuda, T. Nohira, R. Hagiwara and T. Homma, *Metall. Mater. Trans.*
340   *E*, **3**, 145 (2016).

341

342

343 **Table and Figure captions**

344 Table 1 Impurity contents of Si granules obtained after acid leaching, and target levels

345 for primary Si of SOG-Si. The electrolytic reduction of SiO_2 particles was

346 conducted at 0.6 V for 50 h at a liquid Zn cathode in molten $CaCl_2$ at 1123 K.

347 Figure 1 Schematic drawing of SOG-Si production process using electrochemical

348 reduction of SiO_2 powder at a liquid Si–Zn alloy cathode in molten $CaCl_2$.[36,37]

349 Figure 2 Schematic illustration of the electrolysis cell for observation of SiO_2

350 reduction behavior at liquid Zn cathode. (a) Ag^+/Ag reference electrode, (b)

351 Ca^{2+}/Ca dynamic reference electrode on a Mo wire, (c) liquid Zn electrode

352 with Al_2O_3/SiO_2 tube, (d) graphite counter electrode, (e) Al_2O_3 crucible, (f)

353 molten $CaCl_2$, (g) small Al_2O_3 crucible, and (h) liquid Zn.

354 Figure 3 Schematic illustrations of the liquid Zn electrode for (a) cyclic voltammetry

355 and (b) electrolytic reduction of SiO_2 plate.

356 Figure 4 Schematic illustration of the electrolysis cell for the electrolytic reduction of

357 SiO_2 particles. (a) Ag^+/Ag reference electrode, (b) Ca^{2+}/Ca dynamic reference

358 electrode on a Mo wire, (c) W lead wire, (d) graphite counter electrode, (e)

359 Al_2O_3 crucible, (f) molten $CaCl_2$, (g) SiO_2 particle, and (h) liquid Zn.

360 Figure 5 Cyclic voltammograms for liquid Zn electrode with an Al_2O_3 tube or a SiO_2

361   tube (left axis) and for Si plate electrode (right axis) in molten $CaCl_2$ at 1123

362   K. Scan rate: 100 mV s^{-1}.

363 Figure 6 Optical images of the SiO_2 plates after electrolysis at liquid Zn electrode or

364   immersion into liquid Zn for 30 min in molten $CaCl_2$ at 1123 K. (a)

365   potentiostatic electrolysis at 0.9 V, (b) immersion after electrolysis (a), (c)

366   potentiostatic electrolysis at 0.6 V, and (d) immersion after electrolysis (c).

367 Figure 7 (a) An optical image and (b) XRD pattern of the Si granules obtained after

368   acid leaching of Zn ingots. The electrolytic reduction of SiO_2 particles was

369   conducted at 0.6 V for 50 h at a liquid Zn cathode in molten $CaCl_2$ at 1123 K.

370

371

372 **Table 1**. Impurity contents of Si granules obtained after acid leaching, and target levels
373 for primary Si of SOG-Si. The electrolytic reduction of SiO_2 particles was conducted at
374 0.6 V for 50 h at a liquid Zn cathode in molten $CaCl_2$ at 1123 K.

Impurity element, A	Acceptable level for SOG-Si[41], $x_{A(SOG\text{-}Si)}$ / ppmw	Segregation coefficient[7], k°_A	Target level for primary Si[a], $x_{A(primary)}$ / ppmw	Impurity content of Si granules by electrochemical reduction at liquid Zn cathode, x_A / ppmw [b]	Impurity content of Si by direct electrochemical reduction[42], x_A / ppmw [c]
B	0.1–0.3	0.8	0.13–0.38	1.5	2.6
P	0.03–0.04	0.35	0.086–0.4	<0.2	6.4
Al	<0.1	2×10^{-3}	<50	8	600
Ca	<0.2	1.6×10^{-3}	<125	85	5800
Fe	<0.1	8×10^{-6}	<12500	110	30
Ti	$<10^{-3}$	9×10^{-6}	<100	25	19
Zn	—[d]	—[d]	—[d]	6055	2.1

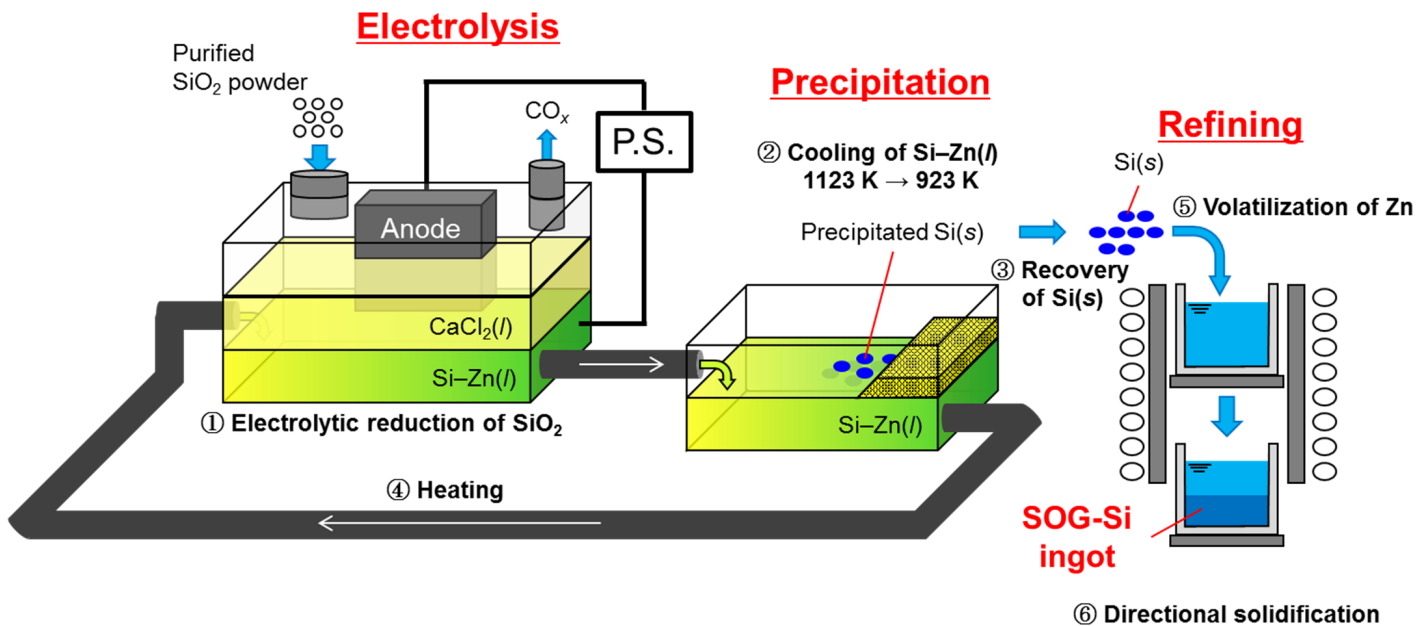375 a: $x_{A(primary)} = x_{A(SOG\text{-}Si)} / k^{\circ}_A$

376 b: Analyzed by ICP-AES
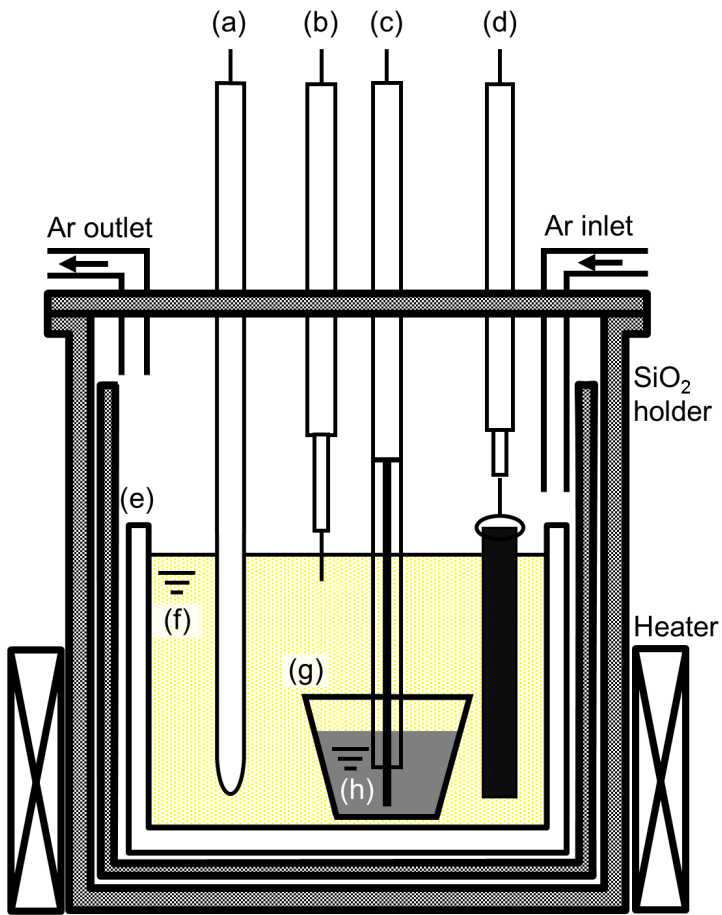
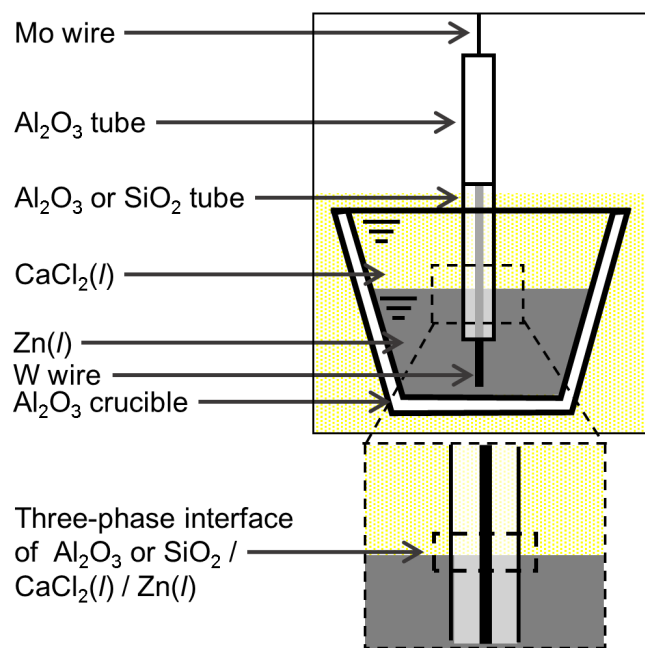377 c: Analyzed by glow discharge-mass spectrometry (GD-MS)

378 d: No data

379

380

Figure 1. Schematic drawing of SOG-Si production process using electrochemical reduction of SiO_2 powder at a liquid Si–Zn alloy cathode in molten $CaCl_2$.[38]
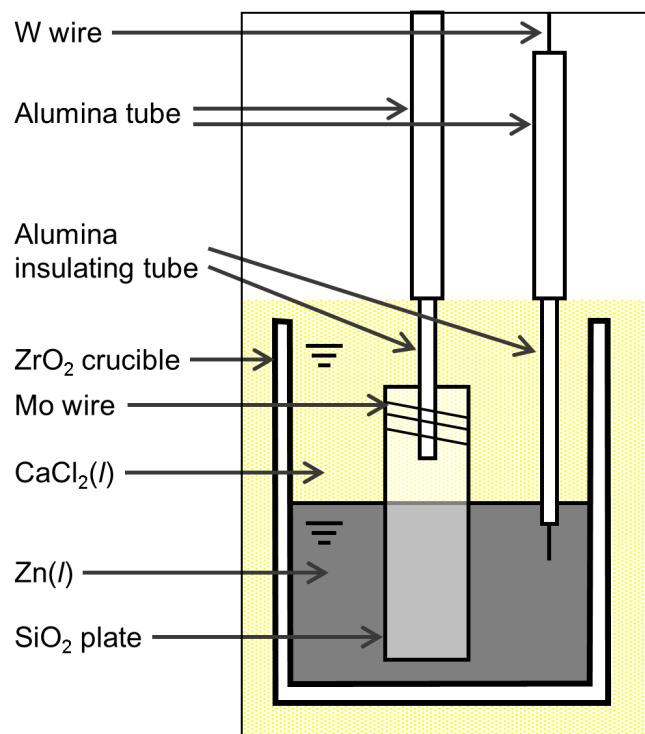
Figure 2. Schematic illustration of the electrolysis cell for observation of SiO_2 reduction behavior at liquid Zn cathode. (a) Ag^+/Ag reference electrode, (b) Ca^{2+}/Ca dynamic reference electrode on a Mo wire, (c)liquid Zn electrode with Al_2O_3/SiO_2 tube, (d) graphite counter electrode, (e) Al_2O_3 crucible, (f) molten $CaCl_2$, (g) small Al_2O_3 crucible, and (h) liquid Zn.

(a)

Mo wire

Al_2O_3 tube

Al_2O_3 or SiO_2 tube

$CaCl_2(l)$

$Zn(l)$
W wire
Al_2O_3 crucible

Three-phase interface
of Al_2O_3 or SiO_2 /
$CaCl_2(l)$ / $Zn(l)$

(b)

W wire

Alumina tube

Alumina
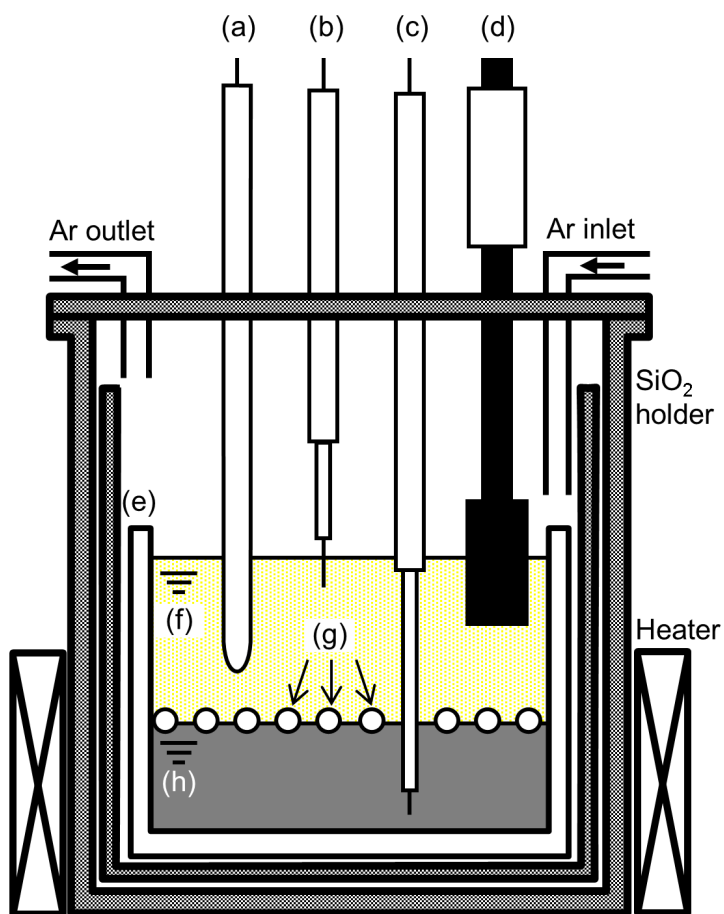insulating tube

ZrO_2 crucible
Mo wire

$CaCl_2(l)$

$Zn(l)$

SiO_2 plate

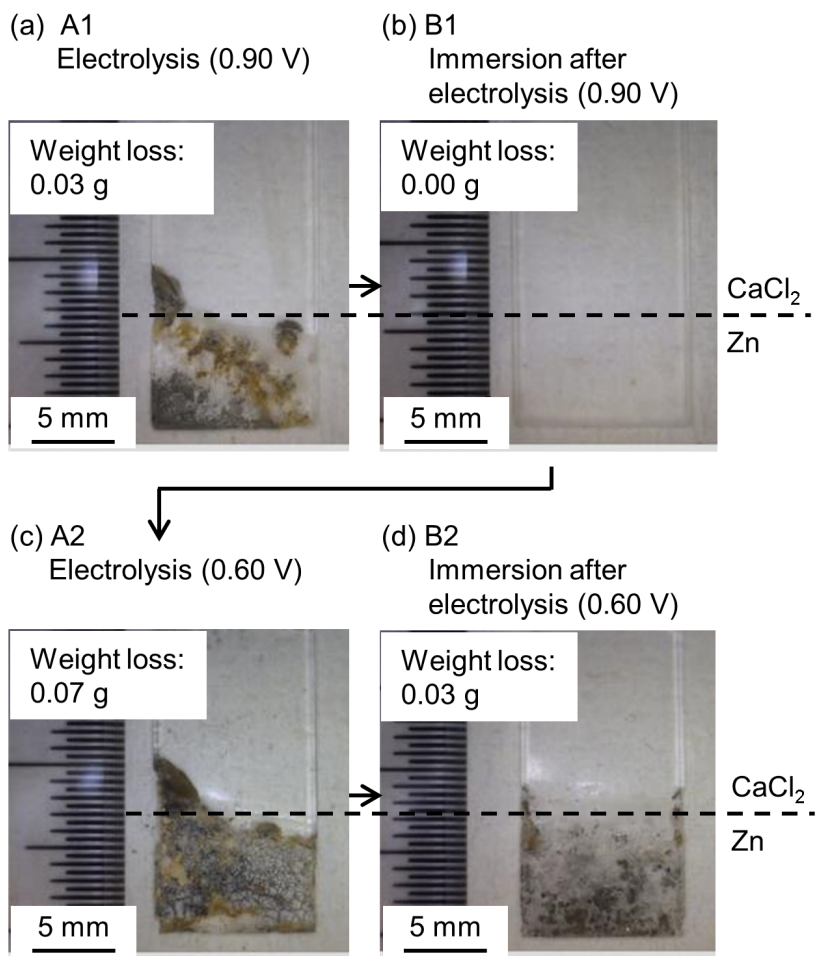**Figure 3**. Schematic illustrations of the liquid Zn electrode for (a) cyclic voltammetry and (b) electrolytic reduction of SiO_2 plate

Figure 4. Schematic illustration of the electrolysis cell for the electrolytic reduction of SiO_2 particles. (a) Ag^+/Ag reference electrode, (b) Ca^{2+}/Ca dynamic reference electrode on a Mo wire, (c) W lead wire, (d) graphite counter electrode, (e) Al_2O_3 crucible, (f) molten $CaCl_2$, (g) SiO_2 particle, and (h) liquid Zn.
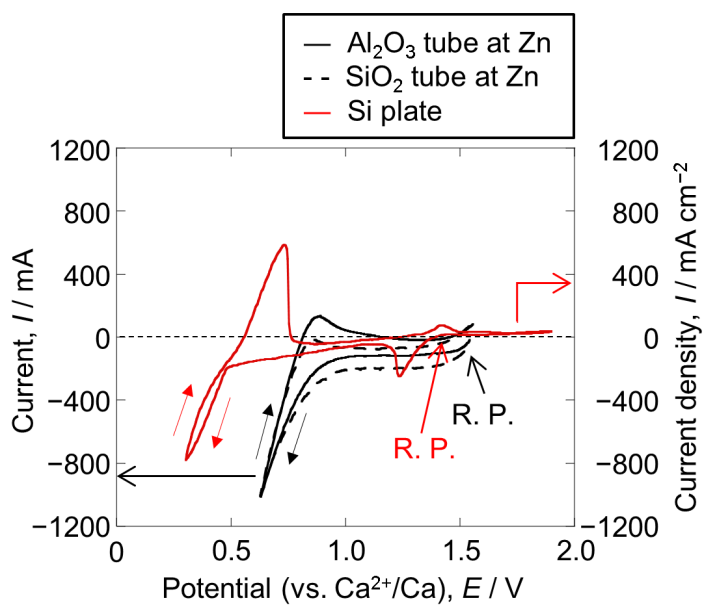
Figure 5. Cyclic voltammograms for liquid Zn electrode with an Al_2O_3 tube or a SiO_2 tube (left axis) and for Si plate electrode (right axis) in molten $CaCl_2$ at 1123 K. Scan rate: 100 mV s^{-1}.

(a) A1
   Electrolysis (0.90 V)

Weight loss: 0.03 g

5 mm

(b) B1
   Immersion after
   electrolysis (0.90 V)

Weight loss: 0.00 g

CaCl$_2$

Zn

5 mm

(c) A2
   Electrolysis (0.60 V)

Weight loss: 0.07 g

5 mm

(d) B2
   Immersion after
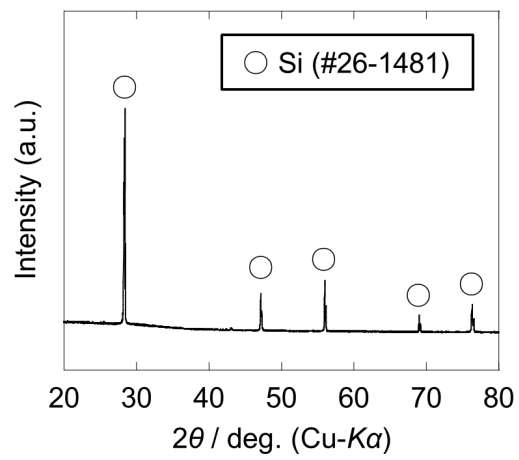   electrolysis (0.60 V)

Weight loss: 0.03 g

CaCl$_2$

Zn

5 mm

Figure 6. Optical images of the SiO$_2$ plates after electrolysis at liquid Zn electrode or immersion into liquid Zn for 30 min in molten CaCl$_2$ at 1123 K. (a) potentiostatic electrolysis at 0.9 V, (b) immersion after electrolysis (a), (c) potentiostatic electrolysis at 0.6 V, and (d) immersion after electrolysis (c).

(a)

1 cm
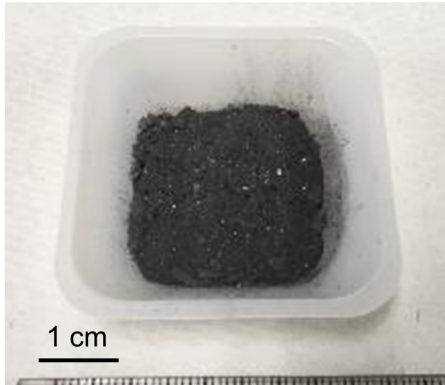
(b)

Figure 7. (a) An optical image and (b) XRD pattern of the Si granules obtained after acid leaching of Zn ingots. The electrolytic reduction of SiO_2 particles was conducted at 0.6 V for 50 h at a liquid Zn cathode in molten $CaCl_2$ at 1123 K.